

A study of non-isothermal kinetics of limestone decomposition in air (O₂/N₂) and oxy-fuel (O₂/CO₂) atmospheres

Luning Tian · Hanping Chen · Zhenhui Chen ·
Xianhua Wang · Shihong Zhang

Received: 25 February 2013 / Accepted: 24 June 2013 / Published online: 27 July 2013
© Akadémiai Kiadó, Budapest, Hungary 2013

Abstract The non-isothermal experiments of limestone decomposition at multi-heating rates in O₂/N₂ and O₂/CO₂ atmospheres were studied using thermogravimetry. The limestone decomposition kinetic model function, kinetic parameters of apparent activation energy (E), and pre-exponential factor (A) were evaluated by Bagchi and Malek method. The results shown that in 20 % O₂/80 % N₂ atmosphere, the limestone decomposed slowly following the contracting sphere volume model controlled by boundary reaction (spherical symmetry) in two stages, and the E increased by about 50 kJ mol⁻¹ in the second decomposition stage. But in 20 % O₂/80 % CO₂ atmosphere, the presence of high-concentration CO₂ significantly inhibited the limestone decomposition, and made the decomposition process occur at high temperature with a rapid rate; the decomposition kinetics was divided into three stages, the first stage was an accelerated decomposition process following the Mampel Power law model with the exponential law equation, the second stage followed the n th order chemical reaction model as an α - t deceleration process, and the third stage belonged to the random nucleation and nuclei growth model with the Avrami–Erofeev equation. And with the heating rate increasing, the reaction order n showed a slight rise tendency. The E was about 1,245 kJ mol⁻¹ in 20 % O₂/80 % CO₂ atmosphere, but was only about 175 kJ mol⁻¹ in 20 % O₂/80 % N₂ atmosphere. The E and A increased markedly in the O₂/CO₂ atmosphere.

Keywords Limestone · TG–DTG · Decomposition kinetics · Malek method · O₂/CO₂ atmosphere

Introduction

The limestone have been applied widely in numerous industrial fields. It can act as raw material in cement industry, fusing agent in metallurgical industry, additive for composite material, SO₂ and CO₂ absorber in coal combustion, and so on [1–4]. But with the rapid development of oxy-fuel combustion technology for CO₂ capture and storage in industry, more limestone will decompose under higher CO₂ concentration atmosphere in industrial application, which will cause a very marked change in decomposition mechanism compared with that in air atmosphere, as shown in previous work [4, 5].

Several researchers have already investigated the decomposition mechanism of limestone in O₂/CO₂ atmosphere, especially in decomposition kinetics [6–13]. Nevertheless, many studies were carried out in lower CO₂ concentration atmosphere, or mainly focused on the values of kinetic parameters, and few studies paid attention to the decomposition mechanism and its difference between O₂/N₂ and O₂/CO₂ atmospheres. Moreover, the single model-fitting method was often used to deduce the kinetic parameters by the non-isothermal experiments in these studies. But in this method, due to the kinetic parameters of mechanism function $f(\alpha)$, E and A are interlinked, each good linear regression of mechanism function $f(\alpha)$ corresponds to one E and A ; besides, there is no ordinary range of the kinetic parameters of limestone decomposition in O₂/CO₂ atmosphere for logical choice at present; so it is difficult to clearly and unambiguously indicate a unique and real decomposition mechanism only by the single

L. Tian · H. Chen (✉) · Z. Chen · X. Wang · S. Zhang
State Key Laboratory of Coal Combustion, Huazhong University
of Science and Technology, Wuhan 430074,
People's Republic of China
e-mail: hp.chen@163.com

model-fitting method. Meanwhile, these studies usually only use one mechanism function to describe the whole decomposition reaction, some possible series–parallel decomposition mechanisms might be neglected in the decomposition process, so it is not feasible for a wide range of solid decomposition [14].

In an attempt to clarify the decomposition mechanism in O₂/CO₂ atmosphere, the non-isothermal experiments were carried out at multi-heating rates by thermogravimetry (TG) in the present work, and the decomposition mechanism was explored by Malek method, which has high-resolving power for kinetic model function. Moreover, some experiments in O₂/N₂ atmosphere as a background also have been done, and its decomposition mechanism was also analyzed by Bagchi method. So, the difference of limestone decomposition mechanism in the two atmospheres can be concluded by comparing them. The results will have great significance for industrial application of limestone in oxy-fuel atmosphere.

Experimental

Material

A sample of limestone was used in decomposition experiments in this study. The limestone was crushed and sieved to obtain the particle size range of less than 63 μm. The chemical composition of the limestone sample is listed in Table 1.

Equipment and procedure

The decomposition behavior of the limestone was studied using a NETZSCH STA 409C TGA. The mass precision of the TG is 5 μg. The temperature was measured by a thermocouple immediately placed under crucible. The high-pure gases of N₂, O₂, and CO₂ were supplied by gas cylinders, and the flow rates of the gases were controlled by

the mass flowmeters. For each experiment, the thin layer of limestone sample was laid out on the bottom of the aluminum oxide crucible of the TG firstly, then the mixed gas was introduced to purge the system, and final the temperature was heated from room temperature to 1,273 K at the different heating rates of 5, 10, and 20 K min⁻¹ in the desired atmosphere. The mass of the sample was kept at 10 mg, and the total flow rate of the mixed gas was fixed at 100 mL min⁻¹.

Kinetic theory

The Malek method, proposed by Malek [15], was introduced to deduce the most probable kinetic model function of limestone decomposition under O₂/CO₂ atmosphere in this study. In the method, a special function $Z(\alpha)$ is defined by combining the differential and integral expressions of the kinetic model function, which can easily be obtained by the TG experimental data. As a completed thermodynamics analysis, it consists of three different methods of the model-free method, master plot method, and model-fitting method, which mostly reduces the range of the possible kinetic model, and besides, there are almost no assumption and approximation, so it is more effective and accurate for deducing the kinetic model. Consequently, it was recommended by ICTAC Kinetics Committee [16] and was often used as a diagnostic means for kinetic model determination [17–20]. The flow chart of the kinetic analysis is shown in Fig. 1.

The procedure of kinetic analysis can be described as follows:

(1) Three model-free methods of Flynn–Wall–Ozawa (FWO) [21], Kissinger–Akahira–Sunose (KAS) [22], and Starink [23], which have no concern with the kinetic model function, were used to calculate the E with a high precision, their expressions are given as follows:

FWO equation:

$$\log \beta = \lg[AE/Rg(a)] - 2.315 - 0.4567 E/RT_P \quad (1)$$

KAS equation:

$$\ln(T_P^2/\beta) = \ln[Eg(a)/AR] + E/RT_P \quad (2)$$

Starink equation:

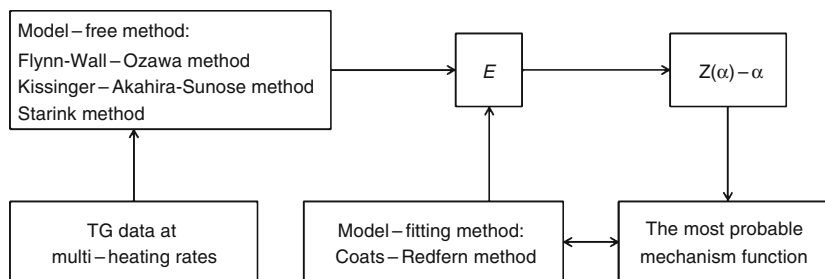
$$\ln(\beta/T_P^{1.8}) = -1.0037E/RT_P + C \quad (3)$$

where α is the fractional conversion according to the formula $\alpha = (m_0 - m_t)/(m_0 - m_\infty)$, m_0 , m_∞ , and m_t are the initial sample mass, final sample mass, and the mass of sample at the time t , respectively; $g(\alpha)$ is the integral expression of kinetic model function; β is the heating rate; R is the gas universal constant; T_P is the maximum decomposition temperature; and C is a parameter that is independent of T_P and β .

Table 1 Chemical composition of limestone sample (XRF analysis)

Composition	Mass fraction/%
Na ₂ O	2.26
Al ₂ O ₃	0.97
SiO ₂	ND
SO ₃	0.18
K ₂ O	ND
CaO	53.16
TiO ₂	ND
Fe ₂ O ₃	0.10
Loss on ignition	42.94

Fig. 1 The flow chart of Malek method



In each method, α should be most similar at the maximum decomposition temperature among the multi-heating rates experiments. For the same α , the plots of $\log\beta$ versus $1/T_P$ (Eq. 1), $\ln T_P^2/\beta$ versus $1/T_P$ (Eq. 2), and $\ln\beta/T_P^{1.8}$ versus $1/T_P$ (Eq. 3) based on the TG data recorded at multi-heating rates should show better linear relationship, and then the values of E can be determined from the slopes of the plotted lines.

(2) Using the E , resulted from above calculation, the experimental $Z(\alpha)$ can be calculated [15]. It is defined as follows:

$$Z(\alpha) = \pi(u)(d\alpha/dt)T/\beta \quad (4)$$

where $u = E/RT$, $\pi(u)$ is an approximation of temperature integral, which can be accurately calculated by the following equation.

$$\pi(u) = (u^3 + 18u^2 + 86u + 96) / (u^4 + 20u^3 + 120u^2 + 240u + 120) \quad (5)$$

where T is the absolute reaction temperature.

Meanwhile, the standardized $Z(\alpha)$ can be obtained by the function as follows:

$$Z(\alpha) = f(\alpha)g(a) \quad (6)$$

where $f(\alpha)$ is the differential form of kinetic model function. So, series standardized $Z(\alpha)$ can be calculated by the kinetic model function expressions of $f(\alpha)$ and $g(\alpha)$. Several common kinetic models and their expressions are given in Table 2 [24]. The standardized $Z(\alpha)$, which is best fitted to the experimental $Z(\alpha)$ can be observed directly by plotting the experimental $Z(\alpha)-\alpha$ and the series standardized $Z(\alpha)-\alpha$ curves; and the $f(\alpha)$ and $g(\alpha)$ corresponded to the standardized $Z(\alpha)$, are the most probable kinetic model functions.

(3) Finally, the most probable kinetic model function, which was deduced in step (2), can be further verified using model-fitting method, such as Coats-Redfern method [25]. The Coats-Redfern method can be deduced as:

$$\ln[g(\alpha)/T^2] = -E/RT + \ln(AR/\beta E) \quad (7)$$

The E and A can be obtained from the slope and intercept of plots of $\ln[g(\alpha)/T^2]$ versus $1/T$, respectively. And, the E can be compared with that derived from model-free methods in step (1).

In conventional air atmosphere, the limestone decomposition mechanism has been investigated widely in the literatures [13, 26–33]. The results shown that the limestone decomposition obeyed the ordinary solid decomposition rule, and the values of E and A , and the kinetic model function $f(\alpha)$ obtained by different kinetic methods were similar. So, authors directly used the Bagchi method and logical choice to analyze the limestone decomposition mechanism in 20 % $O_2/80$ % N_2 atmosphere. The Bagchi method combined the integral and differential methods, the logarithmic forms as follows [34]:

$$\ln[g(\alpha)/(T - T_0)] = \ln(A/\beta) - E/RT \quad (8)$$

$$\ln[(d\alpha/dT)/(E(T - T_0)/RT^2 + 1) \cdot 1/f(\alpha)] = \ln(A/\beta) - E/RT \quad (9)$$

where T_0 is the reaction onset temperature.

The series E and A can be obtained by line plotting $\ln[g(\alpha)/(T - T_0)]$ versus $1/T$ (Eq. 8) and $\ln[(d\alpha/dT)/(E(T - T_0)/RT^2 + 1) \cdot 1/f(\alpha)]$ versus $1/T$ (Eq. 9) with many common kinetic model functions selected, respectively. And, if the most probable kinetic model function is used, the plotted lines should present better linear relationship, and the E and A obtained from the both forms should be comparable with each other.

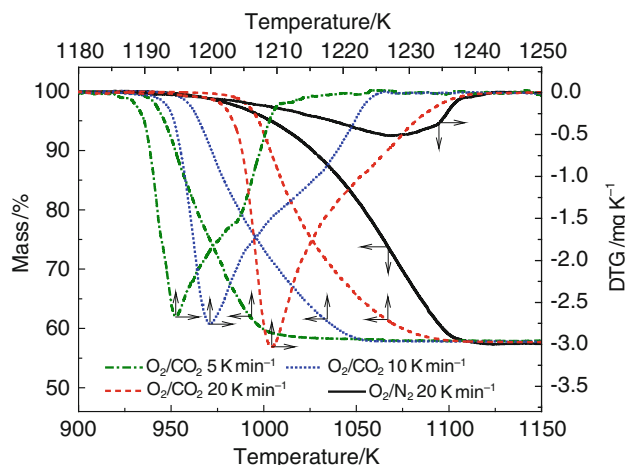
Result and discussion

TG-DTG curves for the limestone decomposition in 20 % $O_2/80$ % N_2 and 20 % $O_2/80$ % CO_2 atmospheres at the different heating rates (5, 10, and 20 $K \min^{-1}$) are shown in Fig. 2. As seen, the initial decomposition temperature increased from 944 K in 20 % $O_2/80$ % N_2 atmosphere to 1,196 K in 20 % $O_2/80$ % CO_2 atmosphere at the heating rate of 20 $K \min^{-1}$. The presence of high-concentration CO_2 significantly inhibited the limestone decomposition, and made the decomposition process occur at high-temperature zone, so the decomposition rate was accelerated, the decomposition time was shortened to 2.05 min from 8.75 min in 20 % $O_2/80$ % N_2 atmosphere. Moreover, the details of decomposition process in two atmospheres have some obvious differences. In 20 % $O_2/80$ % N_2 atmosphere,

Table 2 Several common kinetic model functions for the present analysis

No.	Function name	Differential form $f(\alpha)$	Integral form $g(\alpha)$	Mechanism
1	Jander equation	$3/2(1-\alpha)^{2/3}[1-(1-\alpha)^{1/3}]^{-1}$	$[1-(1-\alpha)^{1/3}]^2$	Three-dimension diffusion, D_3
2	Ginstling–Brounstein equation	$3/2[(1-\alpha)^{-1/3}-1]^{-1}$	$1-2/3\alpha-(1-\alpha)^{2/3}$	Three-dimension diffusion, D_4
3	Valensi equation	$[-\ln(1-\alpha)]^{-1}$	$\alpha + (1-\alpha)\ln(1-\alpha)$	Two-dimension diffusion, D_2
4	Avrami–Erofeev equation	$4/5(1-\alpha)[-\ln(1-\alpha)]^{-1/4}$	$[-\ln(1-\alpha)]^{5/4}$	Random nucleation and nuclei growth, $n = 5/4$
5	Parabola law	$1/2\alpha^{-1}$	α^2	One-dimension diffusion, D_1
6	Avrami–Erofeev equation	$1-\alpha$	$-\ln(1-\alpha)$	Random nucleation and nuclei growth, $n = 1, A_1$
7	Contracting sphere (volume)	$3(1-\alpha)^{2/3}$	$1-(1-\alpha)^{1/3}$	Phase boundary reaction, R_3
8	Contracting cylinder (area)	$2(1-\alpha)^{1/2}$	$1-(1-\alpha)^{1/2}$	Phase boundary reaction, R_2
9	Avrami–Erofeev equation	$2(1-\alpha)[-\ln(1-\alpha)]^{1/2}$	$[-\ln(1-\alpha)]^{1/2}$	Random nucleation and nuclei growth, $n = 1/2, m = 2, A_2$
10	Avrami–Erofeev equation	$3(1-\alpha)[-\ln(1-\alpha)]^{2/3}$	$[-\ln(1-\alpha)]^{1/3}$	Random nucleation and nuclei growth, $n = 1/3, m = 3, A_3$
11	Avrami–Erofeev equation	$4(1-\alpha)[-\ln(1-\alpha)]^{3/4}$	$[-\ln(1-\alpha)]^{1/4}$	Random nucleation and nuclei growth, $n = 1/4, m = 4, A_4$
12	Mampel Power law	1	α	Phase boundary reaction, $n = 1, R_1$
13	Reaction order	$1/3(1-\alpha)^{-2}$	$1-(1-\alpha)^3$	$n = 3$
14	7/4 order	$4/3(1-\alpha)^{7/4}$	$(1-\alpha)^{-3/4}$	Chemical reaction, $n = 7/4$
15	Mampel Power law	$4\alpha^{3/4}$	$\alpha^{1/4}$	$n = 1/4$
16	Mampel Power law	$5\alpha^{4/5}$	$\alpha^{1/5}$	$n = 1/5$
17	2 order	$(1-\alpha)^2$	$(1-\alpha)^{-1}$	Chemical reaction, $n = 2, F_2$
18	3 order	$1/2(1-\alpha)^3$	$(1-\alpha)^{-2}$	Chemical reaction, F_3
19	Avrami–Erofeev equation	$5/2(1-\alpha)[-\ln(1-\alpha)]^{3/5}$	$[-\ln(1-\alpha)]^{2/5}$	Random nucleation and nuclei growth, $n = 2/5$

there are two stages in the decomposition curve, from 944 to 1,068 K is the first stage with slow increase of decomposition rate, and the limestone conversion reached 65 % at the highest decomposition rate, and then the decomposition was completed in the second stage between 1,068 and 1,119 K with a quick decrease of decomposition rate. But in 20 % O₂/80 % CO₂ atmosphere, three distinguished stages are presented in the decomposition curve, a quick increase of decomposition rate occurred in the temperature of 1,196–1,208 K at the first stage, and the conversion reached 18 %; the second stage occurred between 1,208 and 1,216 K with the decomposition rate quick decrease, and the conversion increased from 18 to 64 %; the third stage began at 1,216 K till the decomposition completed at 1,237 K with a slow decrease of decomposition rate. It also can be observed that with the heating rate decrease, the mass loss shifted to lower temperature systematically, while no obvious change showed in its shape. It indicated that the limestone has a similar regular pattern in decomposition at different heating rates in O₂/CO₂ atmosphere. As the heating rate decreased from 20 to 10 and finally to 5 K min⁻¹, the initial decomposition temperature lowered from 1196 to 1191 and 1187 K, but the decomposition time was extended from 2.05 to 3.40 and 4.80 min, respectively. The three

**Fig. 2** TG–DTG curves for the limestone decomposition in 20 % O₂/80 % N₂ and 20 % O₂/80 % CO₂ atmospheres

temperature ranges of limestone decomposition are 1187–1194, 1194–1203, and 1203–1211 K at the heating rate of 5 K min⁻¹, and 1191–1200, 1200–1212, and 1212–1225 K at the heating rate of 10 K min⁻¹.

As described in step (1), the plots of $\log\beta$ versus $1/T_P$ (Eq. 1), $\ln T_P^2/\beta$ versus $1/T_P$ (Eq. 2), and $\ln\beta/T_P^{1.8}$ versus $1/T_P$ (Eq. 3) by TG data at the different heating rates in 20 %

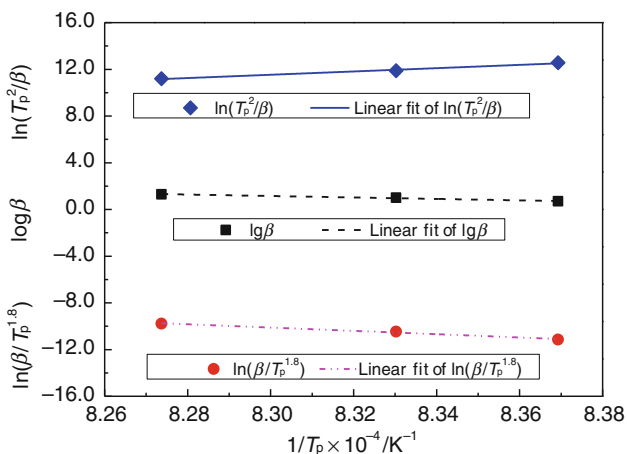


Fig. 3 Fitting curves of $\log\beta$, $\ln T_p^2/\beta$ and $\ln\beta/T_p^{1.8}$ versus $1/T_p$

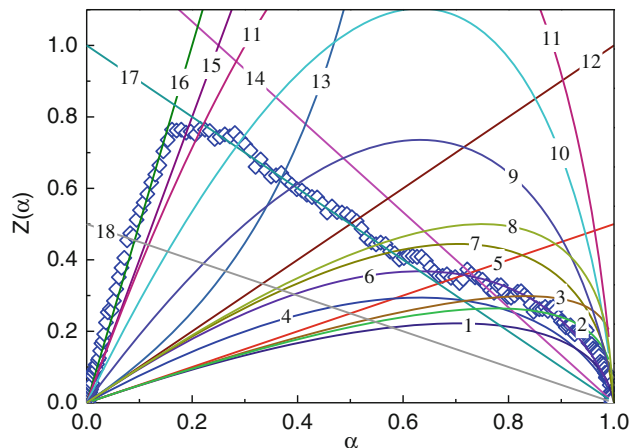


Fig. 5 Fitting curves of experimental $Z(\alpha)-\alpha$ and series standardized $Z(\alpha)-\alpha$ at the heating rate of 10 K min^{-1}

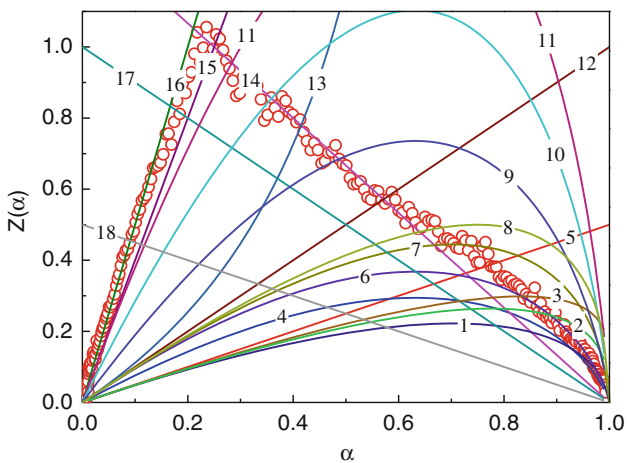


Fig. 4 Fitting curves of experimental $Z(\alpha)-\alpha$ and series standardized $Z(\alpha)-\alpha$ at the heating rate of 5 K min^{-1}

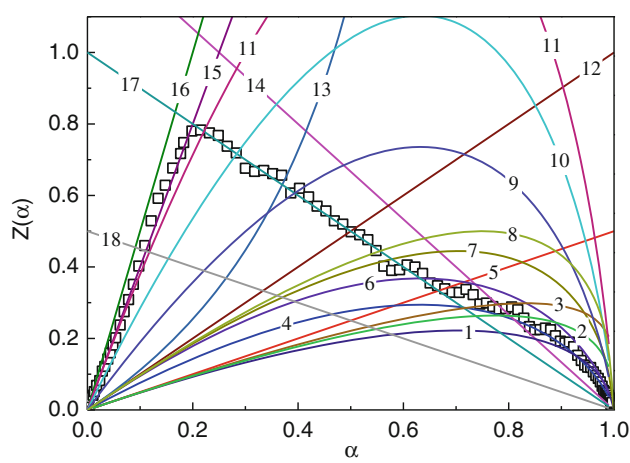


Fig. 6 Fitting curves of experimental $Z(\alpha)-\alpha$ and series standardized $Z(\alpha)-\alpha$ at the heating rate of 20 K min^{-1}

$\text{O}_2/80\% \text{ CO}_2$ atmosphere are shown in Fig. 3. It can be seen that the linear fitting results of three points for each method at different heating rates are better, and then the E for each method was deduced using the slope of the plotted line, there are 1134.33, 1172.87, and 1170.53 kJ mol^{-1} , respectively. The values of E are very similar, especially the last two values, and besides due to the KAS and Starink methods are superior to FWO method [23], the average value of the last two E , 1171.70 kJ mol^{-1} , was used to calculate the experimental $Z(\alpha)$ in the next step in order to ensure the accuracy of calculation.

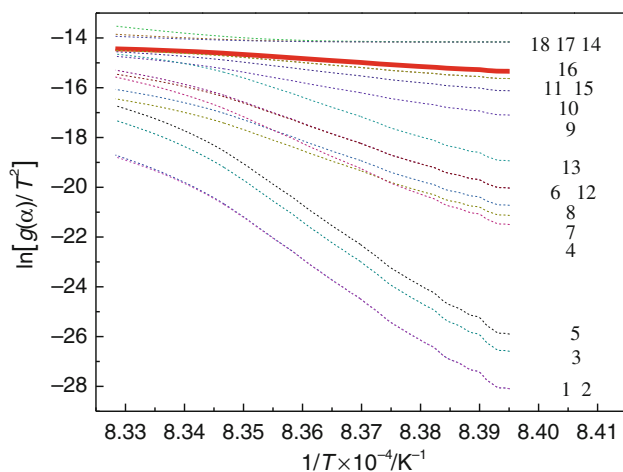
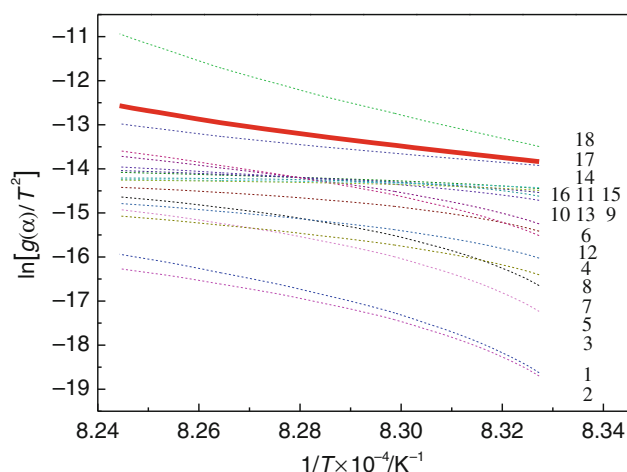
The experimental $Z(\alpha)$ was deduced as described in step (2), and the fitting curves of experimental $Z(\alpha)-\alpha$ and series standardized $Z(\alpha)-\alpha$ at the different heating rates of 5, 10, and 20 K min^{-1} in 20% $\text{O}_2/80\% \text{ CO}_2$ atmosphere are presented in Figs. 4, 5, and 6, respectively. It can be seen that the decomposition kinetics can be well described by three stages, which are fitted to three different

standardized $Z(\alpha)$ at each heating rate, respectively. And they are consistent with that presented in TG curve for decomposition process. The results of the most probable kinetic model functions at different heating rates are summarized in Table 3.

Thus, it can be found that the most probable kinetic model of limestone decomposition is common at the same stage regardless the heating rate. In the first decomposition stage, it follows the Mampel Power law model, the second decomposition stage follows order chemical reaction model, and the third decomposition stage belongs to random nucleation and nuclei growth model. Furthermore, the slight difference of decomposition kinetics among the heating rates is only presented in the reaction order n . At 5 K min^{-1} , the most probable kinetic model functions of the three stages are the exponential law with $n = 1/5$, the n th order reaction with $n = 7/4$, and the Avrami–Erofeev equation with $n = 1$, respectively; but when the heating

Table 3 The results of the most probable kinetic model functions at different heating rates in O₂/CO₂ atmosphere

Heating rate/K min ⁻¹	Stage	Temperature range/K	Function
5	I	1,187–1,194	Mampel Power law ($n = 1/5$)
	II	1,194–1,203	7/4 Order chemical reaction ($n = 7/4$)
	III	1,203–1,211	Avrami–Erofeev equation ($n = 1$)
10	I	1,191–1,200	Mampel Power law ($n = 1/5$)
	II	1,200–1,212	2 Order chemical reaction ($n = 2$)
	III	1,212–1,225	Avrami–Erofeev equation ($n = 1$)
20	I	1,196–1,208	Mampel Power law ($n = 1/4$)
	II	1,208–1,216	2 Order chemical reaction ($n = 2$)
	III	1,216–1,237	Avrami–Erofeev equation ($n = 5/4$)

**Fig. 7** Plots of $\ln[g(x)/T^2]$ versus $1/T$ in the first stage at the heating rate of 10 K min⁻¹**Fig. 8** Plots of $\ln[g(x)/T^2]$ versus $1/T$ in the second stage at the heating rate of 10 K min⁻¹

rate increased to 10 K min⁻¹, the most probable kinetic model function of the second stage is transferred into n th order reaction with $n = 2$; while the heating rate further increased to 20 K min⁻¹, the most probable kinetic model functions of the first and third stages are transferred into the exponential function with $n = 1/4$ and the Avrami–Erofeev equation with $n = 5/4$, respectively. As generally known, the higher limestone decomposition temperature at faster heating rate can accelerate the decomposition rate, while it also enhances the sintering of the calcined product, but in here, the sintering caused by the heating rate increasing can be negligible because of the lower decomposition temperature and the short duration time [35]. So, the slighter increase of the decomposition reaction order n may be contributed to the nonequilibrium conditions of decomposition temperature, which caused by heating rate. In particular, the presence of higher CO₂ concentration can make the decomposition more sensitive to the temperature. The similar phenomenon was also found by Açıkalın [36].

Moreover, in order to further verify the precision of the probable kinetic model function deduced by step (2), series

potential kinetic model functions $g(x)$, including that deduced by step (2), were selected to plot $\ln[g(x)/T^2]$ versus $1/T$ (Eq. 7) curves by Coats–Redfern method. The plots of $\ln[g(x)/T^2]$ versus $1/T$ in the three stages at the heating rate of 10 K min⁻¹ are presented in Figs. 7, 8, and 9.

As seen, the plots of $\ln[g(x)/T^2]$ versus $1/T$ of the most probable kinetic model function deduced by step (2) (No. 16, 17, and 6 in first, second and third stage, respectively) show the best linear relationship in each stage. Meanwhile, the E and A of each stage was obtained from the slope and intercept of the plot of $\ln[g(x)/T^2]$ versus $1/T$ of the most probable kinetic model function, respectively. The apparent activation energy of the whole decomposition process (E_m) can be calculated by weighted mean activation energy method which was proposed by Cumming [37]. The method is described as:

$$E_m = \sum_{i=1}^n E_i \times F_i \quad (10)$$

where E_i and F_i are the activation energy and mass loss fraction in the i stage, respectively. The results are listed in

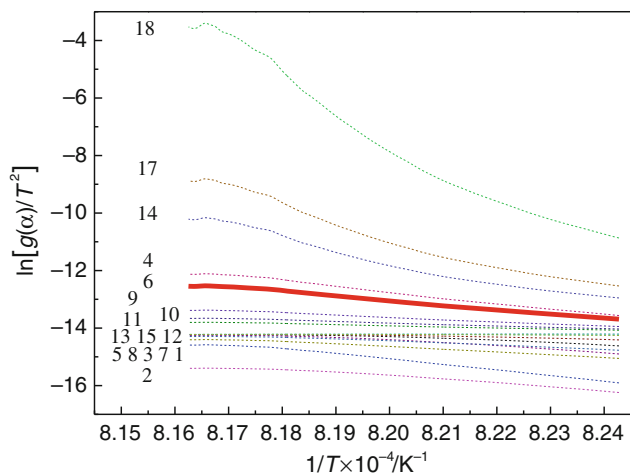


Fig. 9 Plots of $\ln[g(\alpha)/T^2]$ versus $1/T$ in the third stage at the heating rate of 10 K min^{-1}

Table 4. As seen, the values of E and A decrease slightly with the heating rate increasing, it is similar with Rao’s [27] and Bigda and Mianowski’s result [38]. The average value of E at different heating rates is about $1,245 \text{ kJ mol}^{-1}$ in $20 \% \text{ O}_2/80 \% \text{ CO}_2$ atmosphere, and it is almost equal to that calculated previously by three model-free methods.

In conventional air atmosphere, the limestone decomposition mechanism was investigated with Bagchi method. According to the Eqs. (8) and (9), the $\ln[g(\alpha)/(T - T_0)]$ and $\ln[(d\alpha/dT)/(E(T - T_0)/RT^2 + 1) \cdot 1/f(\alpha)]$ were respectively plotted against $1/T$ in $20 \% \text{ O}_2/80 \% \text{ N}_2$ atmosphere at 20 K min^{-1} in the two stages presented in TG curve, and the E and A were obtained from the slopes and intercepts of the plotted lines which shown better linear relationship. Comparing the results of linear fitting, and the E and A deduced by the integral and differential methods, it can be observed that the limestone decomposition in $20 \% \text{ O}_2/80 \% \text{ N}_2$ atmosphere are best fitted to the contracting sphere volume model (R_3) with the differential form $f(a) = 3(1-\alpha)^{2/3}$ and the integral form $g(a) = 1-(1-\alpha)^{1/3}$ in the two stages. The similar result has been reported in the literatures [28, 30, 32].

The linear fitting results, and the values of E and A derived from the R_3 model are listed in Table 5. As shown, the linear fitting results are better, and the values of E and A calculated by the integral and differential methods are most similar, and the E in the second stage increased by about 50 kJ mol^{-1} than that in first stage despite the calculation method. This behavior might be due to that, in the first stage, the effect of heat and mass transfer is limited, and the role of CO_2 diffusion on the decomposition reaction is minor; but with the decomposition continuing, the product layer formed with the calcium oxide recrystallization inhibited the CO_2 diffusion, so the E increases [11].

In comparison with the result obtained in O_2/N_2 and O_2/CO_2 atmospheres, it is indicated that the division of kinetic analysis stages is consistent with that presented in TG curve. In O_2/N_2 atmosphere, the limestone decomposes slowly following the contracting sphere volume model in two stages, the E increases by about 50 kJ mol^{-1} after the decomposition rate reaching the maximum and the decomposition reaction becomes more difficult. In O_2/CO_2 atmosphere, the high CO_2 concentration makes the limestone decompose at high temperature, it decomposes quickly with an acceleration process controlled by nucleation rate in the initial stage. Then, when the decomposition rate reach a maximum, it enters into the $\alpha-t$ deceleration process, which is controlled by the chemical reaction. In the final stage, the decomposition becomes quite difficult, and it is controlled by the formation of crystallization centers and subsequently growth. Moreover, the E and A of limestone decomposition in O_2/CO_2 atmosphere are significantly higher than that in O_2/N_2 atmosphere.

Table 4 Kinetic parameters obtained from the Coats–Redfern method at different heating rates in $20 \% \text{ O}_2/80 \% \text{ CO}_2$ atmosphere

Decomposition stage	I		II		III		$E_m/\text{kJ mol}^{-1}$
	$E/\text{kJ mol}^{-1}$	A/min^{-1}	$E/\text{kJ mol}^{-1}$	A/min^{-1}	$E/\text{kJ mol}^{-1}$	A/min^{-1}	
5	1296.28	$8.09\text{E} + 56$	1283.15	$3.22\text{E} + 56$	1294.92	$5.91\text{E} + 56$	1289.00
10	1223.32	$2.80\text{E} + 53$	1239.51	$2.32\text{E} + 54$	1299.84	$3.21\text{E} + 56$	1248.04
20	1119.42	$2.93\text{E} + 48$	1237.82	$8.09\text{E} + 53$	1215.15	$3.34\text{E} + 52$	1198.34

Table 5 Parameters obtained from Bagchi method in $20 \% \text{ O}_2/80 \% \text{ N}_2$ atmosphere

Decomposition stages	I			II			$E_m/\text{kJ mol}^{-1}$
	$E/\text{kJ mol}^{-1}$	A/min^{-1}	R	$E/\text{kJ mol}^{-1}$	A/min^{-1}	R	
Integral methods	152.34	$1.23\text{E} + 6$	0.9919	202.51	$3.67\text{E} + 8$	0.9976	167.39
Differential methods	165.05	$1.21\text{E} + 7$	0.9980	220.80	$2.20\text{E} + 9$	0.9968	181.78

Conclusions

The non-isothermal thermal kinetics of limestone decomposition in 20 % O₂/80 % N₂ and 20 % O₂/80 % CO₂ atmospheres were determined by Bagchi and Malek method, which can guarantee the precision of the most probably kinetic model functions and kinetic parameters. It was revealed that in 20 % O₂/80 % N₂ atmosphere, the limestone decomposed slowly following the contracting sphere volume model in two stages, which was controlled by boundary reaction (spherical symmetry). But the E increased by about 50 kJ mol⁻¹ in the second decomposition stage because the decomposition reaction became more difficult. In 20 % O₂/80 % CO₂ atmosphere, the presence of high-concentration CO₂ significantly inhibited the decomposition of limestone particle at lower temperature, and made the decomposition to occur at higher temperature with a rapid rate, and the decomposition kinetics can be divided into three stages. The first stage was an accelerated decomposition process following the Mampel Power law model controlled by nucleation rate with exponential law equation. In the second stage, it followed n th order model with an $\alpha-t$ deceleration process controlled by chemical reaction. While in the third stage, belonged random nucleation and nuclei growth model controlled by the formation of crystallization centers and subsequently growth with Avrami–Erofeev equation. And with the heating rate increasing, the n showed a slight rise tendency in general. The E calculated by model-fitting method was mostly equal to that calculated by three model-free methods in 20 % O₂/80 % CO₂ atmosphere, it was about 1,245 kJ mol⁻¹, but was only about 175 kJ mol⁻¹ under 20 % O₂/80 % N₂ atmosphere. The E and A showed a remarkable increase in the O₂/CO₂ atmosphere.

Acknowledgements A financial support of this work by the National Key Technology R&D Program (No. 2010CB227003) and the National Nature Science Foundation of China (No. 51021065 and No. 50930006) are gratefully acknowledged.

References

- Nocuń-Wczelik W, Trybalska B, Żugaj E. Application of calorimetry as a main tool in evaluation of the effect of carbonate additives on cement hydration. *J Therm Anal Calorim.* 2013. doi: 10.1007/s10973-013-2994-6.
- Setta FA, Neville A. Efficiency assessment of inhibitors on CaCO₃ precipitation kinetics in the bulk and deposition on a stainless steel surface (316 L). *Desalination.* 2011;281:340–7.
- Klimova I, Kaljuvee T, Mikli V, Trikkel A. Influence of some lime-containing additives on the thermal behavior of urea. *J Therm Anal Calorim.* 2013;111(1):253–8.
- Chen J, Yao H, Zhang L. A study on the calcination and sulphation behaviour of limestone during oxy-fuel combustion. *Fuel.* 2012;102:386–95.
- Tian LN, Chen HP, Yang HP, Wang XH, Zhang SH. Study of limestone thermal decomposition in O₂/CO₂ atmosphere. In: Qi H, Zhao B, editors. *Cleaner combustion and sustainable world.* Berlin: Springer; 2013. p. 1283–9.
- Criado JM, González M, Málek J, Ortega A. The effect of the CO₂ pressure on the thermal decomposition kinetics of calcium carbonate. *Thermochim Acta.* 1995;254:121–7.
- Khinast J, Krammer GF, Brunner C, Staudinger G. Decomposition of limestone: the influence of CO₂ and particle size on the reaction rate. *Chem Eng Sci.* 1996;51(4):623–34.
- Samtani M, Dollimore D, Alexander K. Thermal decomposition of dolomite in an atmosphere of carbon dioxide: the effect of procedural variables in thermal analysis. *J Therm Anal Calorim.* 2001;65(1):93–101.
- García-Labiano F, Abad A, Diego LF, Gayán P, Adánez J. Calcination of calcium-based sorbents at pressure in a broad range of CO₂ concentrations. *Chem Eng Sci.* 2002;57(13):2381–93.
- Wang Y, Lin S, Suzuki Y. Study of limestone calcination with CO₂ capture: decomposition behavior in a CO₂ atmosphere. *Energy Fuels.* 2007;21(6):3317–21.
- Avila I, Crnkovic PM, Milioli FE, Luo KH. Thermal decomposition kinetics of Brazilian limestones: effect of CO₂ partial pressure. *Environ Technol.* 2011;33(10):1175–82.
- Escardino A, García-Ten J, Saburit A, Feliu C, Gómez-Tena MP. Calcium carbonate decomposition in white-body tiles during firing in the presence of carbon dioxide. *Ceram Int.* 2013;39(6):6379–90.
- Galan I, Glasser F, Andrade C. Calcium carbonate decomposition. *J Therm Anal Calorim.* 2013;111(2):1197–202.
- Burnham AK, Dinh LN. A comparison of isoconversional and model-fitting approaches to kinetic parameter estimation and application predictions. *J Therm Anal Calorim.* 2007;89(2):479–90.
- Málek J, Criado JM. Empirical kinetic models in thermal analysis. *Thermochim Acta.* 1992;203:25–30.
- Vyazovkin S, Burnham AK, Criado JM, Pérez-Maqueda LA, Popescu C, Sbirrazzuoli N. ICTAC Kinetics Committee recommendations for performing kinetic computations on thermal analysis data. *Thermochim Acta.* 2011;520(1–2):1–19.
- Janković B, Mentus S, Jelić D. A kinetic study of non-isothermal decomposition process of anhydrous nickel nitrate under air atmosphere. *Phys B.* 2009;404(16):2263–9.
- Omrani A, Rostami A, Ravari F. Advanced isoconversional and master plot analyses on solid-state degradation kinetics of a novel nanocomposite. *J Therm Anal Calorim.* 2013;111(1):677–83.
- Shuping Z, Yulong W, Mingde Y, Chun L, Junmao T. Pyrolysis characteristics and kinetics of the marine microalgae *Dunaliella tertiolecta* using thermogravimetric analyzer. *Bioresour Technol.* 2010;101(1):359–65.
- Vasić M, Minić DM, Blagojević VA, Minić DM. Mechanism of thermal stabilization of Fe_{89.8}Ni_{1.5}Si_{5.2}B₃C_{0.5} amorphous alloy. *Thermochim Acta.* 2013;562:35–41.
- Flynn JH, Wall LA. A quick, direct method for the determination of activation energy from thermogravimetric data. *J Polym Sci Part B.* 1966;4(5):323–8.
- Kissinger HE. Reaction kinetics in differential thermal analysis. *Anal Chem.* 1957;29(11):1702–6.
- Starink MJ. The determination of activation energy from linear heating rate experiments: a comparison of the accuracy of isoconversion methods. *Thermochim Acta.* 2003;404(1–2):163–76.
- Brown ME. *Introduction to thermal analysis.* Netherlands: Springer; 2004.
- Coats AW, Redfern JP. Kinetics parameters from thermogravimetric data. *Nature.* 1964;201:68–9.
- Ninan KN, Krishnan K, Krishnamurthy VN. Kinetics and mechanism of thermal decomposition of in situ generated calcium carbonate. *J Therm Anal Calorim.* 1991;37(7):1533–43.

27. Rao TR. Kinetics of calcium carbonate decomposition. *Chem Eng Technol.* 1996;19(4):373–7.
28. Maciejewski M. Computational aspects of kinetic analysis. Part B: The ICTAC Kinetics Project—the decomposition kinetics of calcium carbonate revisited, or some tips on survival in the kinetic minefield. *Thermochim Acta.* 2000;355(1–2):145–54.
29. Ar İ, Doğu G. Calcination kinetics of high purity limestones. *Chem Eng J.* 2001;83(2):131–7.
30. Escardino A, Garcia-Ten J, Feliu C. Kinetic study of calcite particle (powder) thermal decomposition: Part I. *J Eur Ceram Soc.* 2008;28(16):3011–20.
31. Anbalagan G, Rajakumar PR, Gunasekaran S. Non-isothermal decomposition of Indian limestone of marine origin. *J Therm Anal Calorim.* 2009;97(3):917–21.
32. Marinoni N, Allevi S, Marchi M, Dapiaggi M. A kinetic study of thermal decomposition of limestone using in situ high temperature X-ray powder diffraction. *J Am Chem Soc.* 2012;95(8):2491–8.
33. Georgieva V, Vlaev L, Gyurova K. Non-isothermal degradation kinetics of CaCO_3 from different origin. *J Chem.* 2013;2013:12.
34. Bagchi TP, Sen PK. Combined differential and integral method for analysis of non-isothermal kinetic data. *Thermochim Acta.* 1981;51(2–3):175–89.
35. Chen CM, Zhao CS, Liang C, Pang KL. Calcination and sintering characteristics of limestone under O_2/CO_2 combustion atmosphere. *Fuel Process Technol.* 2007;88(2):171–8.
36. Açıklım K. Pyrolytic characteristics and kinetics of pistachio shell by thermogravimetric analysis. *J Therm Anal Calorim.* 2012;109(1):227–35.
37. Cumming JW. Reactivity of coals via a weighted mean activation energy. *Fuel.* 1984;63(10):1436–40.
38. Bigda R, Mianowski A. Influence of heating rate on kinetic quantities of solid phase thermal decomposition. *J Therm Anal Calorim.* 2006;84(2):453–65.